J Intell Robot Syst (2014) 73:289–308
DOI 10.1007/s10846-013-9973-9

A HIL Testbed for Initial Controller Gain Tuning of a Small Unmanned Helicopter

Sepehr P. Khaligh · Alejandro Martínez · Farbod Fahimi · Charles Robert Koch

Received: 1 September 2013 / Accepted: 18 September 2013 / Published online: 18 October 2013

Abstract A Hardware-In-The-Loop (HIL) testbed design for small unmanned helicopters which provides a safe and low-cost platform to implement control algorithms and tune the control gains in a controlled environment is described. Specifically, it allows for testing the robustness of the controller to external disturbances by emulating the hover condition. A 6-DOF nonlinear mathematical model of the helicopter has been validated in real flight tests. This model is implemented in real-time to estimate the states of the helicopter which are then used to determine the actual control signals on the testbed. Experiments of the longitudinal, lateral and heading control tests are performed. To minimize the structural stress on the fuselage in case of controller failure or a subsystem malfunction, a damping system with a negligible parasitic effect on the dynamics of the helicopter around hover is incorporated. The HIL testbed is capable of testing the helicopter in hover, as well as on any smooth trajectories such as cruise flight, figure-8, etc. Experimentally tuning the controller on the HIL testbed is described and results in a controller which is robust to the external disturbances, and achieves an accuracy of ±2.5 cm in the position control on the longitudinal and lateral trajectory tracking, and ±5 deg accuracy around the yaw axis on the heading trajectory tracking.

Keywords Unmanned helicopter · Hardware-In-The-Loop (HIL) testbed · Control gain tuning · External disturbances

S. P. Khaligh (✉) · A. Martínez · C. R. Koch
Department of Mechanical Engineering,
University of Alberta,
Edmonton, AB T6G 2G8, Canada
e-mail: sepehr.khaligh@ualberta.ca

C. R. Koch
e-mail: bob.koch@ualberta.ca

F. Fahimi
Department of Mechanical and Aerospace Engineering, University of Alabama in Huntsville,
Huntsville, AL 35899, USA

1 Introduction

Unmanned aerial systems are a very active research area due to their broad range of applications [1–5]. Researchers are working on different types and sizes of Unmanned Aerial Vehicle (UAV) platforms, from Micro-Air-Vehicles (MAV) including Quadrotors and micro fixed-wing aircrafts, to Ultra-High-Endurance (UHE) vehicles [6–12]. During the process from conceptual design to fabrication and deployment, a number of technical and theoretical challenges must be solved. UAV control is a challenging multidisciplinary problem that combines control with aerodynamics. Particularly challenging are

Vertical Take-off and Landing (VTOL) platforms among which unmanned helicopters are one of the most demanding.

Due to their inherent instability, nonlinearity, non-minimum phase behavior, and aerodynamic complexity, unmanned helicopters offer tremendous challenges during the control design and implementation phases [13–18]. In-flight tuning of control parameters of small unmanned helicopters is difficult due to their high manoeuvrability and inherent instability properties, and catastrophic damage in the event of a crash. Although computer simulation is extremely useful to test controller performance, an intermediate step between simulation and real flight test allows for implementation issues on the real hardware to be tested.

From simple testbed configurations to complete and costly Hardware-In-The-Loop (HIL) simulation testbeds, a variety of systems have been reported in the literature. A three Degree of Freedom (DOF) testbed for quadrotor attitude stabilization is described in [19] and it consists of a single pole fixed to the ground at one end and a spherical joint allowing 3-DOF about the Euler angles at the other end. The quadrotor is then stabilized by implementing a robust fuzzy controller. The single pole structure is simple and affordable, but it may not be suitable for larger helicopters which are capable of generating considerable lift and moments.

Another approach is presented in [20] and [21] for a 3-DOF motion control of a setup [22]. This system consists of an arm with a platform on one end and two propellers mounted to the platform to emulate a helicopter. The platform itself has 1-DOF motion about pitch axis and the whole arm is balanced with a counterweight at the other end. Thus the arm is free to move in both elevation and azimuthal directions. In addition, the main arm is equipped with a motorized lead screw, allowing the motion of a mass attached to it. In this way, controllable and quantifiable disturbances can be generated. This setup is useful to study nonlinearities, uncertainties, unmodeled dynamics, etc. as in [20], where adaptive output feedback control is used to reject parameter uncertainties and unmodeled dynamics including actuator saturation. Similarly, an adaptive controller to reject nonlinearities and unmodeled dynamics, and provide a robust control solution is proposed in [21]. However, due to the constraints imposed by this system, it does not represent the response of an actual helicopter. For example, the emulated helicopter cannot perform a free translational motion and its Center of Gravity (CG) is constrained to the surface of a sphere.

To test the landing phase in difficult terrains for helicopters, a 5-DOF HIL testbed is developed in [23]. The system is composed of a 5-DOF test platform, a computer that controls the motion of the testbed and an avionics box. The testbed itself can perform linear absolute motion about x, y and z axis and two angular motion, pan and tilt, relative to the platform in which the helicopter's avionics is attached. The testbed in conjunction with the avionics box are used to emulate the helicopter's motion based on the dynamic model, which provides high repeatability during emulated flight trajectory tracking in a controlled environment. This is an effective solution to the problem of landing on difficult terrains, but it is inadequate for those cases in which unmodeled dynamics or unexpected disturbance of the helicopter are present since the actual helicopter is not included.

Another approach that involves a 5-DOF testbed, is presented in [24] which is a customized version of the Whitman [25]. It is composed of a central shaft with an arm attached to it, allowing for azimuthal and elevation motion. At the end of the arm there is a platform allowing rotation in the three Euler directions. The helicopter cannot perform a free translational motion but constrained motion is allowed by the testbed. A fuzzy logic based algorithm is used to control the helicopter on the testbed. Although the testbed works well with the fuzzy logic control as a non model-based algorithm, it is difficult to use this testbed for model-based control. This is due to the constraints imposed by the testbed on the translational motion of the helicopter which modifies the real unconstrained helicopter response. For example, to increase the altitude of the helicopter on the testbed, its Center of Gravity (CG) must move towards the center of the testbed, and CG is constrained to the surface of a sphere and cannot move freely in space.

A 6-DOF indoor stand is presented in [26] for control studies. The testbed is composed of a linkage mechanism that allows for the free motion of the helicopter in a $2 \times 2 \times 2$ m^3 cube. The symmetrical geometry of the mechanism makes it equivalent to a concentrated mass, and the design of the stand allows for the free 6-DOF motion of the helicopter. However, the mechanism attached to the helicopter constantly alters the 3D location of its CG during the operation, and the added dynamics of the testbed might not be negligible.

Another approach is presented in [27] to test the performance of MAVs in near-Earth environments such as forests or in an urban environment. The design concept is a 6-DOF gantry attached to a non-flying mockup of a MAV. The mockup emulates the motion of the MAV using a high-fidelity mathematical model and a control system that moves the gantry accordingly. The test rig is especially equipped for emulating adverse weather conditions such as fog, rain and dust. Although the concept provides a suitable solution for testing MAVs in the Near-Earth environments, it might not be suitable for the cases dealing with unmodeled dynamics since the actual vehicle is not included.

In this work, to facilitate tuning of control gains as well as testing both model-based and non-model-based controllers against external disturbances for small unmanned helicopters, a low-cost HIL testbed is designed, built, and experimentally tested. By implementing a 6-DOF nonlinear mathematical model of the helicopter, the developed HIL simulation generates the actual motion of the vehicle and calculates the states. Then, an onboard computer determines the control signals to the actual helicopter mounted on the testbed. A 2-DOF testbed setup configurable for independently testing the longitudinal, lateral, and heading control is presented. In the designed testbed, the added dynamics due to the testbed itself is negligible. Using this testbed, the robustness of the controller can be tested against external disturbances by manually or mechanically disturbing the helicopter during the operation and its performance can be tuned. This can be difficult to do in a real flight test. A special damping system is designed to emulate the hover maneuver. It exerts no damping in hover, which allows for the hover control testing without any interference from the damping system. If the helicopter deviates from its nominal hover position, the damping increases and smoothly slows down the motion. This minimizes the structural stress on the fuselage and rotor mechanism for large deviations. Moreover, the designed HIL testbed allows for testing the helicopter in hover, as well as any smooth trajectories, such as the forward flight, figure-8, etc.

The remainder of this paper is organized into sections. Section 2 describes the architecture of the HIL simulation testbed design. In Section 3 the testbed modeling is described. The control design is presented in Section 4. Finally, the experimental results from the longitudinal, lateral, and heading tests are presented in Section 5, and Section 6 has conclusions.

2 Hardware-in-the-Loop (HIL) Simulation

Controller gain tuning is often part of a control design and requires the system to be in operation during the tuning process. For small unmanned helicopters, in-flight gain tuning is potentially risky and expensive due to the high manoeuvrability and internal instability properties of these vehicles which may result in a crash during the tuning process. In order to facilitate safe tuning of control gains and to test the controller against external disturbances in a controlled environment, a Hardware-In-The-Loop (HIL) testbed design for small unmanned helicopters has been developed and is shown in Fig. 1.

Schematics of the testbed from the front and side views are shown in Fig. 2. This testbed is a 2-DOF system composed of a long pole to raise the helicopter off the floor to eliminate the ground effect and a headpiece. The pole is anchored to the ground. The headpiece is connected to the pole through a set of thrust roller bearings which allows for the rotation of the head with respect to the pole around the vertical Z-axis. The headpiece itself is composed of: a U-shape aluminum plate, two arms, a damping cylinder, a counter balance weight, and one stopper on each side. The helicopter is mounted on Arm 1 which is connected to Arm 2 through two ball bearings on the U-shape plate. This allows for the rotation of the

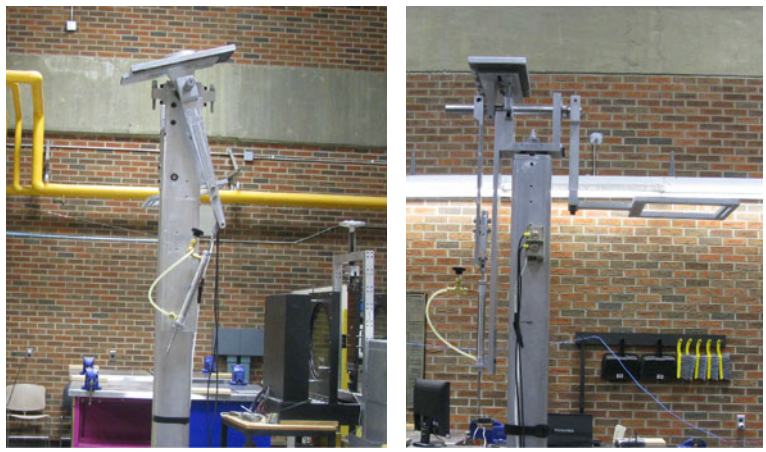

Fig. 1 Front and side views of the HIL testbed

helicopter around the horizontal X-axis. To allow independent testing of the longitudinal/lateral motion a mechanical device restricts the rotation of the headpiece around the vertical axis. Two adjustable hard stoppers restrict the rotation around the X-axis to ±30 deg. In the event of controller malfunction, a nonlinear passive damping system, shown from the front view in Fig. 2, prevents the helicopter from hitting the hard stops at a large angular speed.

The damping system is composed of a double acting cylinder fully filled with a light oil NUTO A10. An oil line with an adjustable needle valve connects the cylinder's inlet to its outlet and makes a closed path of oil. Since the cylinder is double acting and its rod extends from both ends of the barrel, it allows for the continuous flow of oil between the chambers and does not require any oil reservoir.

When testing the helicopter around hover on the testbed, the cylinder is vertical and creates a negligible damping due to the vertical mechanism geometry. As the helicopter deviates from hover the cylinder angle relative to the vertical pole increases and the damping increases in a nonlinear manner. Once the control gains are properly tuned for hover the damping cylinder is removed and the controller is tested against external disturbances.

The counter weight is chosen to precisely balance the arms to mimic hover condition and the mechanism shown in Fig. 2 is designed such that the CG of the helicopter is aligned with the horizontal X-axis which is the axis of rotation in roll and pitch tests.

The goal of the designed HIL simulation testbed is to safely test and tune the longitudinal, lateral and heading controller of the helicopter

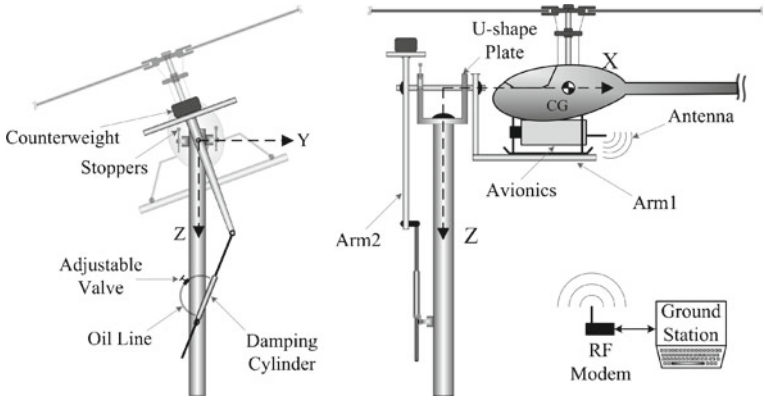

Fig. 2 HIL Testbed schematic of front and side views

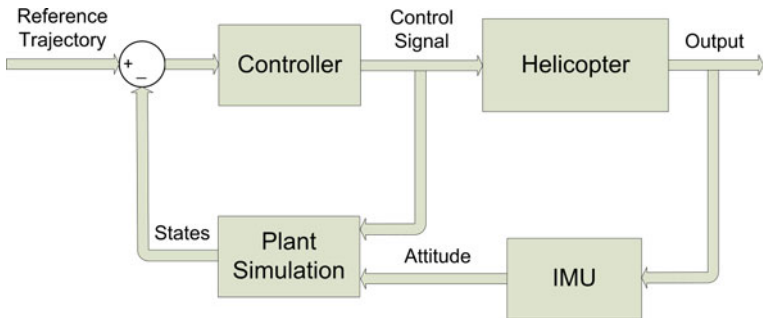

Fig. 3 Block diagram of the HIL simulation

in real-time on the ground. In addition, it allows for testing the robustness of the controller against external disturbances. Using this testbed the helicopter can be disturbed during operation and the performance of the controller can be tuned. Furthermore, the testbed is designed such that the added dynamics due to the testbed itself is negligible. The testbed can also be used for testing the avionics of small helicopters on the ground. The disadvantage of this HIL system is that all degrees of freedom cannot be tested simultaneously and they must be tested one at a time. Simultaneous testing of all DOFs of the helicopter requires a more complex setup, in which the added dynamics due to the testbed itself might not be negligible.

The block diagram of the HIL simulation is shown in Fig. 3. The controller block represents the onboard embedded control system which calculates and outputs control signals to the actual servos of the helicopter. The helicopter block in the diagram represents the physical helicopter to be tested. The IMU block represents the Inertial Measurement Unit which determines the actual attitude of the helicopter including the Euler angles and their rates at every sampling time. However, as the helicopter is fixed on the testbed, its position and velocity are determined using the plant simulation model. The plant simulation generates the actual motion of the helicopter using its 6-DOF nonlinear mathematical model. Using the control signals calculated by the controller and the current IMU outputs as inputs, the position and velocity of the simulated helicopter are determined at every sampling time by integrating the 6-DOF equations of motion. The calculated states of the helicopter are then used as the feedback signal to the controller for the next sampling time computations. This HIL is implemented in real-time at a sample rate of 50 Hz using xPC Target [28].

This HIL testbed allows for testing the helicopter not only in hover but also for smooth trajectories, such as the cruise flight, figure-8, etc. For instance, lateral control of the helicopter in a figure-8 trajectory can be implemented on the testbed by allowing the physical rotation of the vehicle only around the roll axis (the x-axis shown in Fig. 2) and then calculating the actual motion of the rest of the DOFs in the plant simulation using its 6-DOF nonlinear mathematical model. Since the physical motion of these DOFs are mechanically restricted on the testbed, and the controller is controlling all 6-DOFs of the helicopter, the generated control signal for them are not physically realized on the actual helicopter. Rather, some of these signals are applied to the simulated helicopter model in the plant simulation while the control signal corresponding to the moving DOF is physically applied to the actual helicopter.

3 Testbed Modeling

Using the Newton-Euler equations of motion, the attitude dynamic model of the helicopter and the testbed can be written as

$$\frac{d\boldsymbol{\omega}}{dt} = (\boldsymbol{I} + \boldsymbol{I}_{tb})^{-1}(\mathbf{M} + \mathbf{M_{tb}}) - (\boldsymbol{I} + \boldsymbol{I}_{tb})^{-1}(\boldsymbol{\omega} \times (\boldsymbol{I} + \boldsymbol{I}_{tb})\boldsymbol{\omega}) \quad (1)$$

where, the angular velocity of the helicopter in the body coordinates is denoted by $\boldsymbol{\omega} = [p\ q\ r]^T$, and $\boldsymbol{I}$ and $\boldsymbol{I}_{tb}$ are the moment of inertia tensors of

the helicopter and the testbed, respectively. The moment of inertia due to the components on the testbed that are moving with the helicopter is almost ten times smaller than that of the helicopter in pitch and five times smaller in roll thus are neglected. **M** is the total moment vector applied to the helicopter from the main and tail rotor blades. The parasitic moment vector applied from the testbed to the helicopter is denoted by $\mathbf{M_{tb}}$. This is due to the damping effect of the cylinder, and its magnitude can be written as

$$\begin{aligned} M_{tb} &= -rb\dot{\ell}\cos\left(\frac{\pi}{2}-\theta-\alpha\right) \\ &= -rb\dot{\ell}\sin(\theta+\alpha) \end{aligned} \tag{2}$$

where, b is the damping coefficient of the cylinder. $\dot{\ell}$ is the rate at which the cylinder elongates and is calculated by taking time derivative of the loop closure equation in the complex plane for the planar mechanism "OBC". The following vector relation holds for the mechanism shown in Fig. 4

$$\mathbf{l}-\mathbf{r}=\mathbf{h} \tag{3}$$

The loop closure equation can be written in the complex plane as

$$\ell\, e^{j(\frac{\pi}{2}-\alpha)} - r\, e^{-j(\frac{\pi}{2}-\theta)} = jh \tag{4}$$

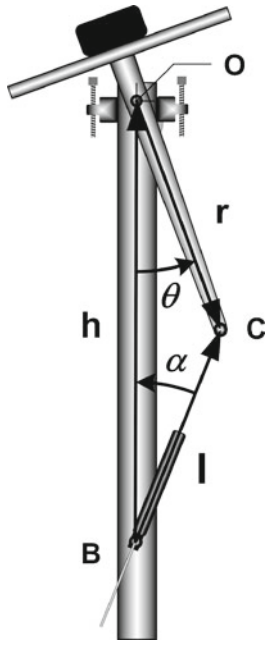

Fig. 4 Testbed mechanism

where $j=\sqrt{-1}$. Using Euler's formula results in

$$\ell(\sin(\alpha)+j\cos(\alpha)) - r(\sin(\theta)-j\cos(\theta)) = jh \tag{5}$$

Rearranging Eq. 5 results in

$$\ell\sin(\alpha) - r\sin(\theta) = 0 \tag{6}$$

$$\ell\cos(\alpha) + r\cos(\theta) = h \tag{7}$$

Since the testbed is designed to test the helicopter around hover, the angles θ and α are small. Assuming small angles for θ and α in Eqs. 6 and 7 results in

$$\ell\alpha - r\theta = 0 \tag{8}$$

$$\ell + r = h \tag{9}$$

Then, differentiating from Eqs. 6 and 7 with respect to time and assuming small angles results in

$$\dot{\ell}\alpha + \ell\dot{\alpha} - r\dot{\theta} = 0 \tag{10}$$

$$\dot{\ell} - \ell\alpha\dot{\alpha} - r\theta\dot{\theta} = 0 \tag{11}$$

Rearranging Eq. 8 to 11 results in:

$$\alpha = \frac{r\theta}{h-r} \tag{12}$$

$$\dot{\ell} = r\dot{\theta}\frac{(\alpha+\theta)}{1+\alpha^2} \tag{13}$$

Since α is small around hover, Eq. 13 can be simplified to

$$\dot{\ell} = r\dot{\theta}(\alpha+\theta) \tag{14}$$

Substituting Eqs. 12 and 14 into Eq. 2 results in a parasitic testbed moment of

$$M_{tb} = -\frac{h^2r^2}{(h-r)^2}b\theta^2\dot{\theta} \tag{15}$$

Equation 15 shows that the damping moment, M_{tb}, generated by the cylinder around hover is negligible when θ is small. However, if the helicopter on the testbed becomes unstable, it starts deviating from hover and the damping moment given in Eq. 15 increases in a nonlinear manner.

This is used to prevent the helicopter from abrupt motion or hitting the hard end stops.

4 Control Design

The control algorithm used in this paper is based on the Sliding Mode Control (SMC) which is robust to external disturbances. The sliding mode control design method in this section follows [29]. As SMC is a model-based algorithm, it requires an accurate 6-DOF nonlinear mathematical model of the helicopter.

Helicopters have two underactuated DOFs, as they are 6-DOF systems controlled by only four active control inputs. To design SMC the dynamic model of the helicopter is modified to have the same number of inputs and outputs. This can be achieved by using the Control Point approach which is summarized next.

For helicopters with a flybar (such as the one tested here) the roll and pitch DOFs are stabilized by the passive control of the flybar. A point on the main hub axis other than the CG is chosen as the point of control. Therefore, any deviations from the desired attitude would result in the deviation of this point from its desired position. This point is called the "Control Point" (CP). In general, a controller designed based on this approach actively controls the 3D position of the control point together with the heading of a helicopter with a flybar while the flybar passively stabilizes the roll and pitch DOFs. A more detailed discussion of this method can be found in [30].

Using the Control Point approach, the dynamic model of the helicopter can be written in an input-output control-affine form as follows,

$$\ddot{\boldsymbol{y}}_{4\times1} = \boldsymbol{f}(\boldsymbol{y}, \dot{\boldsymbol{y}})_{4\times1} + \boldsymbol{b}(\boldsymbol{y}, \dot{\boldsymbol{y}})_{4\times4}\boldsymbol{u}_{4\times1} \tag{16}$$

where $\boldsymbol{f}(\boldsymbol{y}, \dot{\boldsymbol{y}})$ includes the nonlinear centrifugal and coriolis terms, $\boldsymbol{b}(\boldsymbol{y}, \dot{\boldsymbol{y}})$ is the control gain matrix. $\boldsymbol{u} = [\delta_{lon}, \delta_{lat}, \delta_{col}, \delta_{ped}]^T$ is the control input with the longitudinal and lateral cyclic, collective and tail pitch angles, respectively. $\boldsymbol{y} = [x_{cp}, y_{cp}, z_{cp}, \psi_{cp}]^T$ is the control output and includes the 3D position of a point on the main hub axis above the CG together with the heading of the helicopter.

To design a sliding mode controller four asymptotically stable equations are defined

$$\boldsymbol{s} = \dot{\boldsymbol{e}} + \boldsymbol{\lambda}\, \boldsymbol{e} = \boldsymbol{0} \tag{17}$$

where $\boldsymbol{s}$ is the surface function, $\boldsymbol{e} = \boldsymbol{y} - \boldsymbol{y}^d$ is the error of the control output from its desired value and $\boldsymbol{\lambda} = \text{diag}_{4\times4}(\lambda_1, \lambda_2, \lambda_3, \lambda_4)$, with all the components to be strictly positive, is the convergence rate. Rewriting Eq. 17 in the following form

$$\boldsymbol{s} = \dot{\boldsymbol{y}} - \boldsymbol{s_r} \tag{18}$$

where $\boldsymbol{s_r} = \dot{\boldsymbol{y}}^d - \boldsymbol{\lambda e}$. Since the surface defined by Eq. 17 is asymptotically stable, if the system is controlled such that $\boldsymbol{s}$ reaches zero and stays at zero at all times, the output error $\boldsymbol{e}$, will converge to zero. In order for $\boldsymbol{s}$ to be zero the following Lyapunov candidate function is defined

$$V = \frac{1}{2}\boldsymbol{s}^T\boldsymbol{s} \tag{19}$$

In order for $\dot{V} \leq 0$ the control input is calculated as

$$\boldsymbol{u} = \hat{\boldsymbol{b}}^{-1}(-\hat{\boldsymbol{f}} + \dot{\boldsymbol{s}}_{\boldsymbol{r}} - \boldsymbol{K}\, sat(\boldsymbol{\Phi^{-1}s})) \tag{20}$$

where $\boldsymbol{K} = \text{diag}_{4\times4}(k_1, k_2, k_3, k_4)$ is the sliding mode control gain matrix and $\hat{\boldsymbol{b}}$ and $\hat{\boldsymbol{f}}$ are the system matrices calculated using nominal values of the model parameters. To avoid chattering a continuous saturation function with the boundary layer thickness $\boldsymbol{\Phi}$ is used in Eq. 20.

In the absence of any model mismatch and uncertainties in Eq. 16, selection of any positive definite matrix $\boldsymbol{K}$ in Eq. 20 would result in the convergence of the error $\boldsymbol{e}$ to zero. The presence of external disturbances or parameter uncertainties requires the components of $\boldsymbol{K}$ to be large enough such that the following sliding condition is satisfied,

$$\dot{V} \leq -\boldsymbol{\eta}|\boldsymbol{s}| \tag{21}$$

where $\boldsymbol{\eta}$ has strictly positive components and determines the convergence rate to the surface. This

condition results in the following formula for the sliding control gain

$$(1-\Delta_{ii})k_i + \sum_{j\neq i}^{4} \Delta_{ij}k_j = F_i + \eta_i$$

$$+ \sum_{j=1}^{4} \Delta_{ij}|\dot{s}_{ri} - \hat{f}_j|,\ i = 1, ..., 4 \tag{22}$$

where $\boldsymbol{F}$ and $\boldsymbol{\Delta}$ are the uncertainty bound matrices as

$$|\boldsymbol{f} - \hat{\boldsymbol{f}}| \leq \boldsymbol{F} \tag{23}$$

$$\boldsymbol{b} = (\mathbf{I}_{4\times 4} + \boldsymbol{\delta})\hat{\boldsymbol{b}}, \quad |\boldsymbol{\delta}| \leq \boldsymbol{\Delta} \tag{24}$$

By knowing the uncertainty bounds $\boldsymbol{F}$ and $\boldsymbol{\Delta}$ and solving Eq. 22 for K_i's at each sampling time it is guaranteed that the control outputs will follow their desired trajectories [29].

5 Experimental Results

The airframe to be tested in this work is the Evolution Ex helicopter shown in Fig. 5, which is an electric model helicopter with a 2 m blade span and payload of 10 kg. The Avionics box of the helicopter is shown in Fig. 6 and includes: a PC-104 computer as the real-time embedded controller, a Crossbow NAV440 GPS-Aided Inertial Measurement Unit (IMU), an Xstream RF modem for communicating with the ground station, a Servo Switch Card (SSC) for switching between the manual radio and automatic control and a microcontroller for the battery voltage and current monitoring.

Fig. 5 Evolution EX helicopter

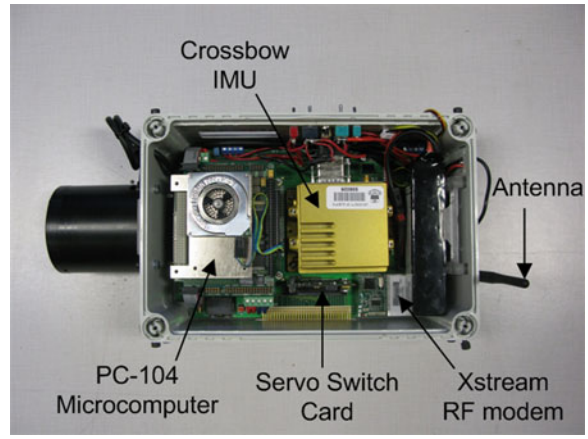

Fig. 6 Avionics of the helicopter

The ground station computer communicates with the Avionics on the helicopter using a pair of RF modem receivers and allows for online updating and uploading the control gains as well as monitoring the attitude, rotor speed, and voltage and current of the batteries. The communication interface of the ground station is shown in Fig. 7.

5.1 Tuning the Control Gains

Using the testbed to tune the control gains in hover for longitudinal, lateral and heading motion the following steps are taken:

1) One of the longitudinal or lateral motion is chosen and the helicopter is placed on the testbed accordingly.
2) It is assumed that the positions of the CP corresponding to the other motion and the heading of the helicopter are all equal to the desired ones. This is to facilitate the process of finding the appropriate control gains corresponding to a motion. For example, to obtain the gains of the longitudinal motion, the lateral and vertical positions of the control point and the heading angle of the helicopter are assumed to have the corresponding values in hover.
3) At hover, tune the controller gains to stabilize the helicopter to get initial gains. Some trial and errors might be required to find the appropriate gains.

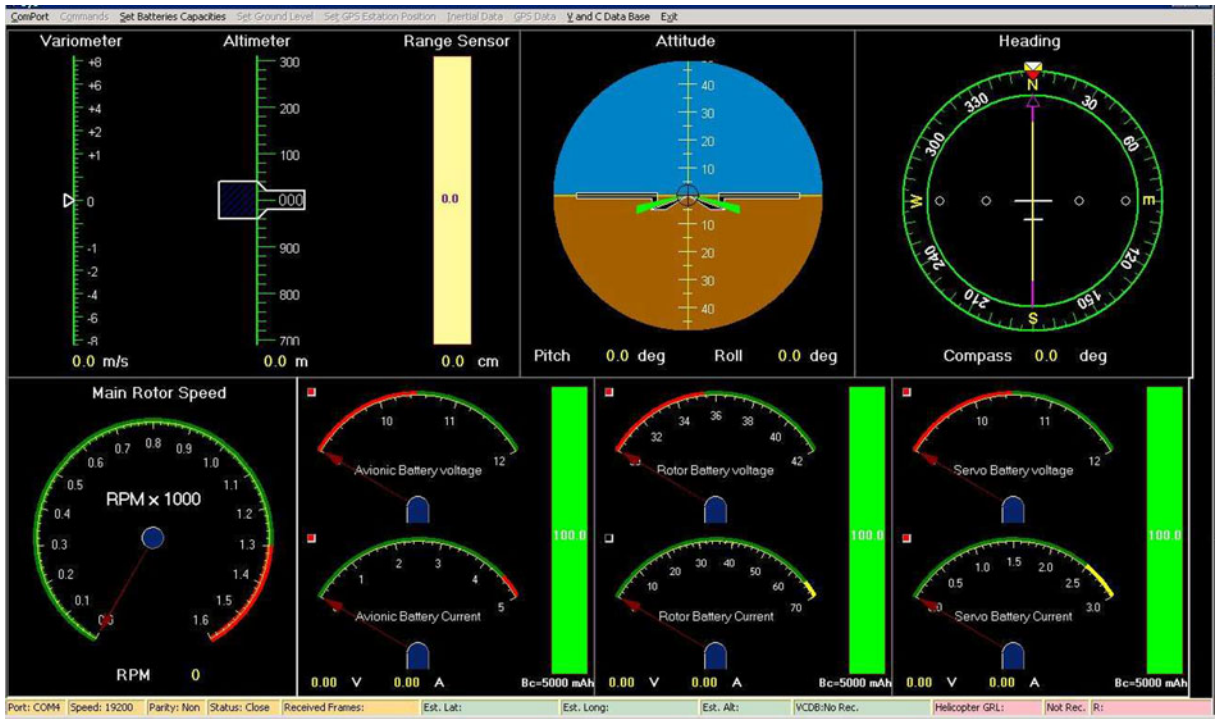

Fig. 7 Ground station interface

4) With the control gains set at initial values for hover, remove the damping cylinder and repeat the test to fine tune the controller. Then the helicopter is intentionally disturbed from the hover position and the gains are further tuned such that the appropriate response rejection of the helicopter to external disturbances is achieved. The applied disturbance that can be rejected depends on the size of the helicopter and the range of the aerodynamic moments that the blades can generate.
5) Once the control gains for the longitudinal motion are properly tuned they are updated in the control program and the controller is tuned for the lateral motion. To do this the helicopter is placed as shown in Fig. 16 and the steps 1 to 4 above are repeated to obtain the gains for the lateral motion.
6) Once the control gains of the longitudinal and lateral motion are tuned, the helicopter is placed on the testbed as shown in Fig. 23, and the procedure is again repeated to tune the controller for the heading motion.

Table 1 Control gains obtained from the HIL experiments

Gain	Description	Longitudinal	Lateral	Heading
λ	Convergence rate	2.5	2.5	2.5
F	Bound on f	10	15	1
Δ	Bound on b	0.5	0.5	0.5
η	Surface reach time	1	1	1
Φ	Boundary layer thickness	0.8	0.6	1

The control gains for the longitudinal, lateral, and heading motion, obtained using the above procedure are listed in Table 1.

5.2 Longitudinal Control Experiment

The longitudinal control of the helicopter is tested by placing it on the testbed as shown in Fig. 8. Only the longitudinal motion of the helicopter is tested in this experiment, since the physical rotation around the vertical axis of the testbed is mechanically restricted. Although the helicopter is physically restricted to rotate only around the pitch axis in this experiment, the controller is con-

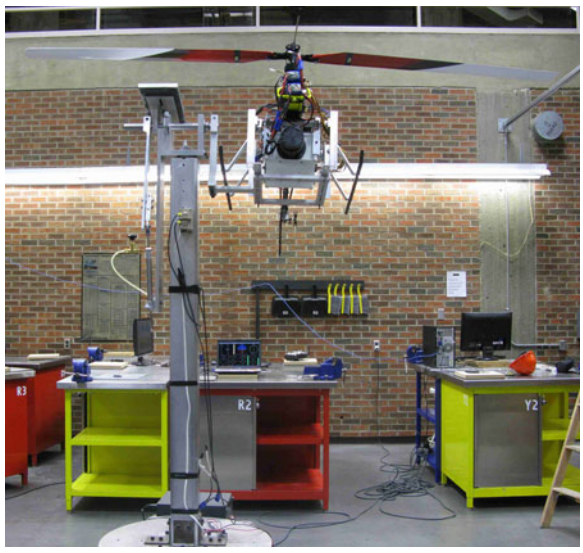

Fig. 8 HIL testbed setup for the longitudinal control in hover

trolling all 6-DOFs of the helicopter. The actual motion of the helicopter is calculated using the 6-DOF nonlinear model of the helicopter at every sampling time as shown in Fig. 3.

The CG of the helicopter shown in Fig. 8 is aligned with the axis of rotation. Depending on the size of the blades and the maximum rolling and pitching moments generated the needle valve on the damping cylinder shown in Fig. 2 is adjusted to prevent sudden movements that could damage the vehicle during tuning. Then once the desired gains are set, the damping effects are reduced by adjusting the needle valve and then by removing the cylinder to test the controller subject to the imposed external disturbances without damping.

The Control Point (CP) is chosen to be 3 m above the CG on the main hub axis of the Evolution EX helicopter. Although the Control Point approach, described in Section 4, is used in this paper to tune the gains of the Sliding Mode controller, the testbed can be used for tuning any controller designed using any approach. In the following the controller is tested for hover, forward, sideways and figure-8 trajectory tracking and the corresponding results are presented.

5.2.1 Hover-Longitudinal

To emulate hover a constant collective pitch of $\delta_{col} = 5.6$ deg for Evolution EX at hover is used throughout this experiment. This is due to the fact that the vertical motion of the helicopter is mechanically restricted on the testbed, and the generated control signal for the heave motion is not physically applied to the actual helicopter, but is applied to the simulated helicopter model in the plant simulation as shown in the block diagram of Fig. 3. In this experiment the control signal

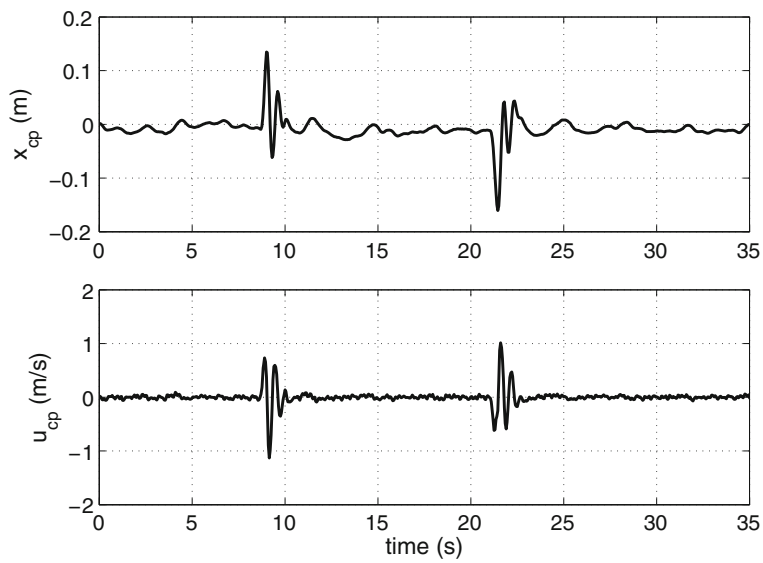

Fig. 9 Position and velocity of the control point in the hover control—the two overshoots at 8.5 and 21 s are due to the intentional external disturbances

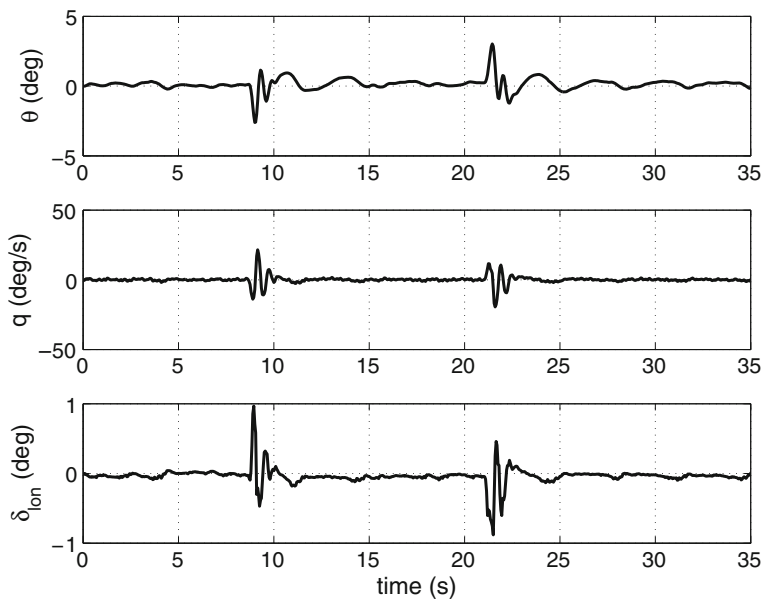

Fig. 10 Closed-loop pitch response and longitudinal cyclic input in the hover control and in the presence of intentional external disturbances

corresponding to the pitch motion is physically applied to the actual helicopter.

The closed-loop response of the control point position and velocity along the longitudinal axis is shown in Fig. 9 and the pitch angle, pitch rate, and the longitudinal cyclic command are shown in Fig. 10. During the experiment the helicopter was intentionally disturbed two separate times at 8.5 and 21 s, by manually exerting a moment of approximately 2.5 Nm to the fuselage for about 1 s to tilt it away from the level position. As shown in Figs. 9 and 10, the controller responds by actuating

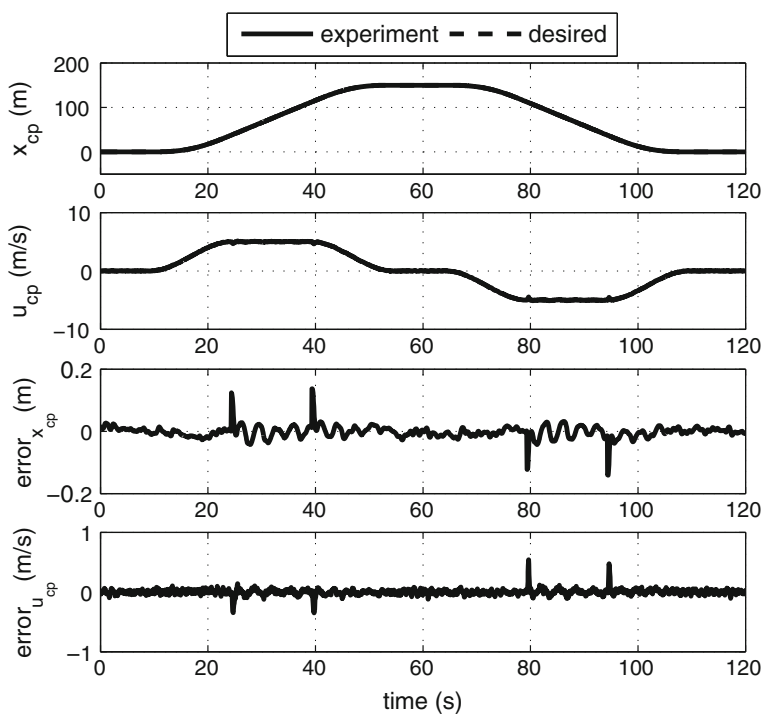

Fig. 11 Position and velocity of the control point and error in the forward flight trajectory tracking control

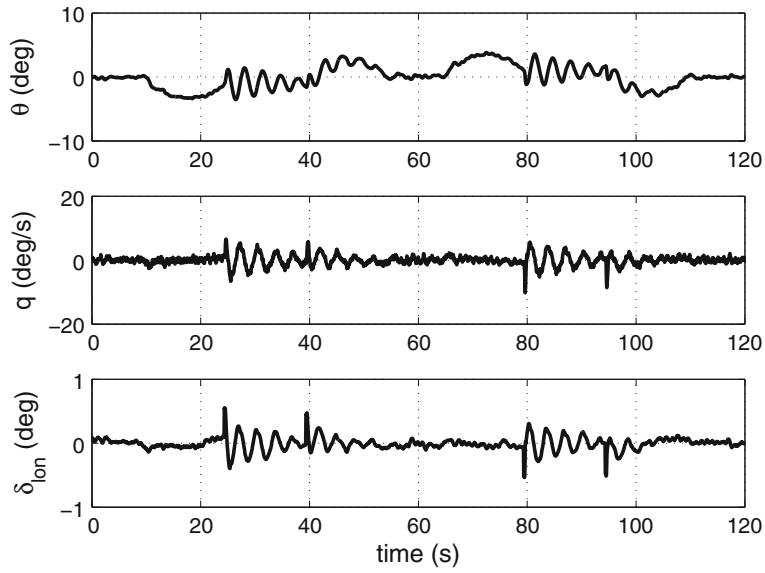

Fig. 12 Closed-loop pitch response and longitudinal cyclic input in the forward flight trajectory tracking control

the longitudinal cyclic pitch of the main rotor blades to reject the disturbances and maintain the zero position and velocity of the control point along the longitudinal axis with a mean absolute error of 1.5 cm and 5.1 cm/s respectively. Also, the steady state pitch angle and pitch rate are close to zero which show that the controller stabilizes the longitudinal motion of the helicopter in the presence of the external disturbances.

5.2.2 Forward Flight-Longitudinal

The desired forward trajectory shown in Fig. 11 is composed of two successive acceleration/deceleration cycles. The trajectory initially starts from the zero position of the CP at hover, and after 15 s accelerates to reach the speed of 5 m/s. It continues the cruise flight at this speed for 15 s, then decelerates again until it comes to a stop at 150 m from the starting point. This cycle is repeated in the backward flight until it reaches the starting point.

The trajectory tracking results are shown in Fig. 11. In addition, the error in both position and velocity are also plotted in Fig. 11—note the y-axis scale of the position and velocity errors in this figure. The results show that the controller successfully tracks the desired trajectory with a mean absolute error of 1.8 cm in position and 3.9 cm/s in velocity. The pitch angle, pitch rate and the longitudinal cyclic command are shown in Fig. 12 and are close to zero which indicates that the controller stabilizes the longitudinal motion of the helicopter in the forward flight.

5.2.3 Figure-8 Trajectory-Longitudinal

The trajectory shown in Fig. 13 is composed of a 5th-order polynomial section followed by a figure-8 section. The trajectory starts in hover at $x_{cp} =$ 10 m and stays in hover for 10 s. Then, the CP moves on a 5th-order polynomial section and after 20 s it enters a figure-8 section. Finally, after

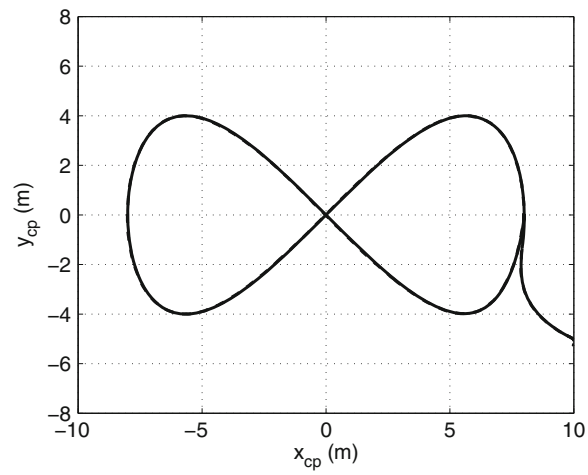

Fig. 13 Figure-8 desired trajectory

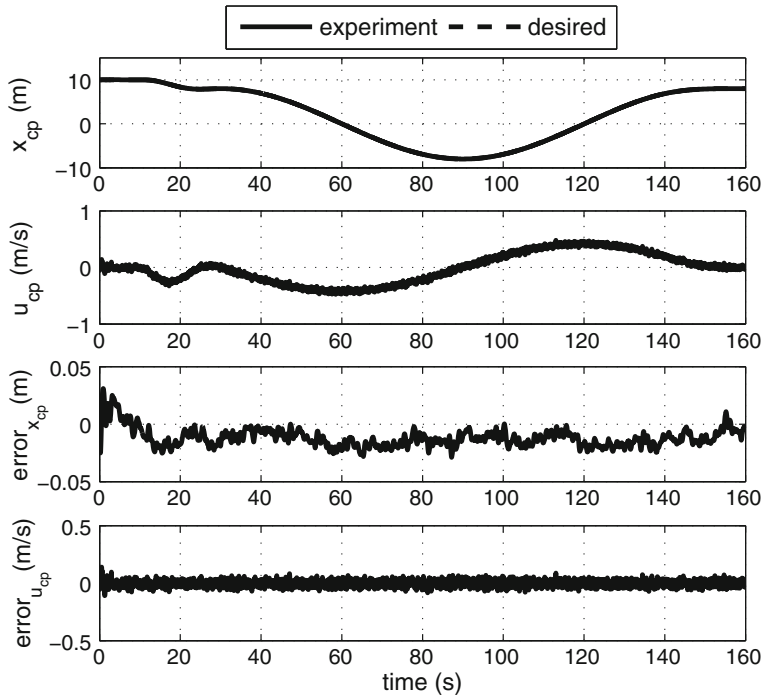

Fig. 14 Position and velocity of the control point and error in the figure-8 trajectory tracking control

ending the figure-8 section it comes to a stop at $t = 160$ sec and $x_{cp} = 8$ m. The yaw angle is considered constant at zero in this trajectory.

Similar to the forward flight trajectory tracking, controlling the helicopter on the figure-8 trajectory also requires controlling the other DOFs and since the helicopter is physically allowed to rotate only around the pitch axis in this experiment, only the longitudinal cyclic pitch command is physically applied to the actual helicopter.

A comparison between the desired and experiment results in Fig. 14 shows that the controller successfully tracks the desired trajectory with a mean absolute error of 1.7 cm in position, and

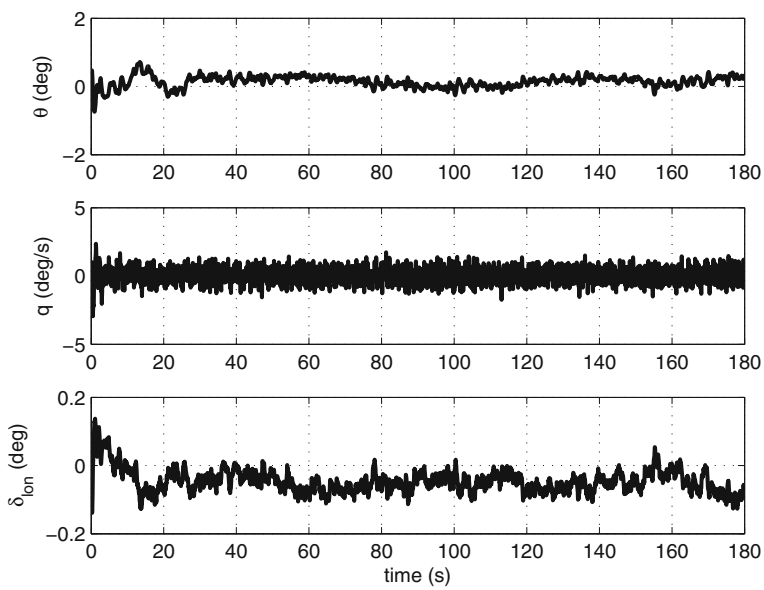

Fig. 15 Closed-loop pitch response and longitudinal cyclic input in the figure-8 trajectory tracking control

Fig. 16 HIL testbed setup for the lateral control in hover

2.1 cm/s in velocity. The pitch angle and pitch rate results in Fig. 15 show that the controller stabilizes the longitudinal motion of the helicopter in the figure-8 trajectory tracking.

5.3 Lateral Control Experiment

The lateral control of the helicopter is tested by securing it on the testbed as shown in Fig. 16. In this position the CG of the helicopter is aligned with the axis of rotation as in the side view of Fig. 16. Similar to the previous test, once the main rotor reached the nominal speed of about 1100 rpm and the collective pitch of 5.6 deg at hover the controller is switched on for the lateral control of the helicopter.

5.3.1 Hover-Lateral

The closed-loop response of the control point position and velocity along the lateral axis is shown in Fig. 17 while the roll angle, roll rate and the lateral cyclic command are shown in Fig. 18. During the experiment the helicopter is intentionally disturbed three times at 7, 13 and 19 s by applying a moment of approximately 2.5 Nm to the fuselage for approximately 1 s to cause it to tilt away from its desired position in hover. This test demonstrates that the controller adjusts the lateral cyclic pitch of the main rotor blades to reject the disturbances and maintain the zero position and velocity of the control point along the lateral axis with a mean absolute error of 1.9 cm and 9.4 cm/s respectively. The results in Fig. 18 show that the desired steady state roll angle is not zero but is −6 deg. This is due to the fact that in hover, the helicopter must have a slight bank angle to compensate for the tail rotor thrust and the desired steady state roll rate is zero. This shows that the controller stabilizes the lateral motion of the

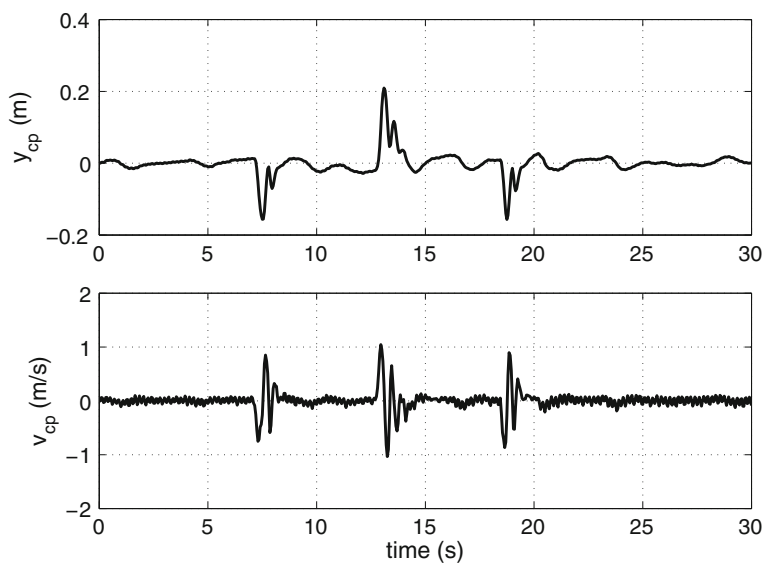

Fig. 17 Position and velocity of the control point in the hover control—the three overshoots at 7, 13 and 19 s are due to the external disturbances

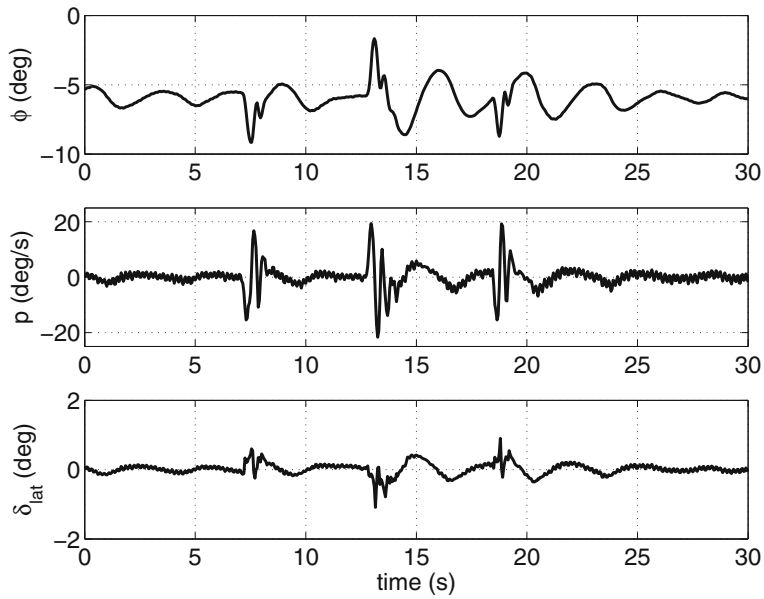

Fig. 18 Closed-loop roll response and lateral cyclic input in the hover control and in the presence of external disturbances

helicopter in the presence of intentional external disturbances.

5.3.2 Sideways Flight-Lateral

Similar to the forward test in Section 5.2.2, the desired sideways trajectory shown in Fig. 19, is composed of two successive acceleration/deceleration cycles. The trajectory tracking results in Figs. 19 and 20 show that the controller tracks the desired trajectory with a mean absolute error of 2.3 cm in position and 5.9 cm/s in velocity when stabilizing the lateral motion of the helicopter in sideways trajectory tracking.

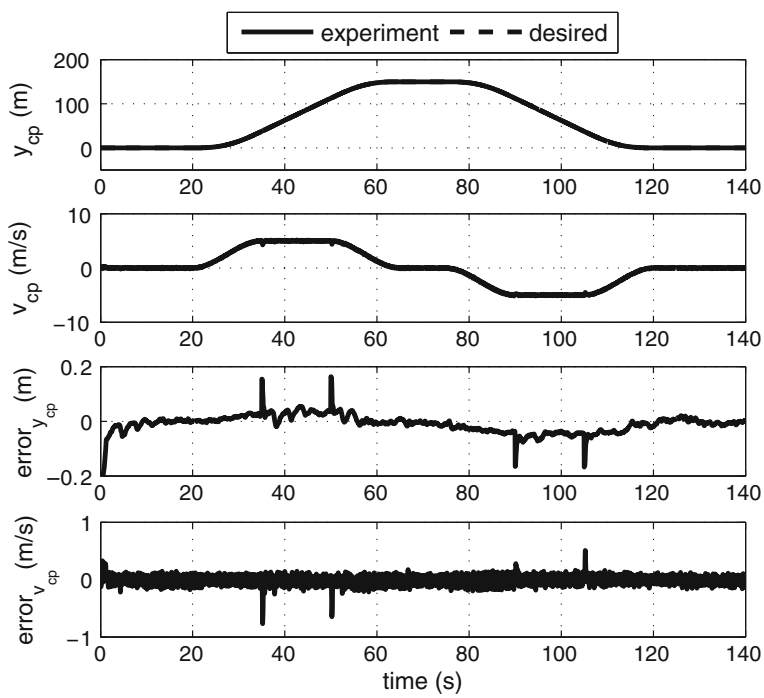

Fig. 19 Position and velocity of the control point and error in the sideways flight trajectory tracking control

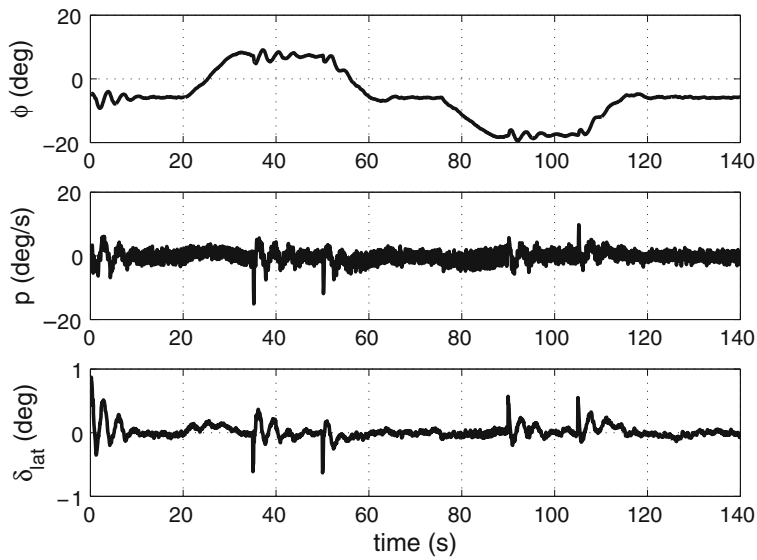

Fig. 20 Closed-loop roll response and lateral cyclic input in the sideways flight trajectory tracking control

5.3.3 Figure-8 Trajectory-Lateral

The figure-8 trajectory is shown in Fig. 13. As previously described, this trajectory is composed of a 5th-order polynomial and a figure-8 section. It starts at $y = -5$ m in hover and stays in hover for 10 s. Then, the CP moves on a 5th-order polynomial section for 20 s before entering a figure-8 section. Finally, it comes to a stop at $t = 160$ s and $y_{cp} = 0$ m after completing the figure-8 section.

The lateral motion results of Figs. 21 and 22 show that the controller successfully tracks the

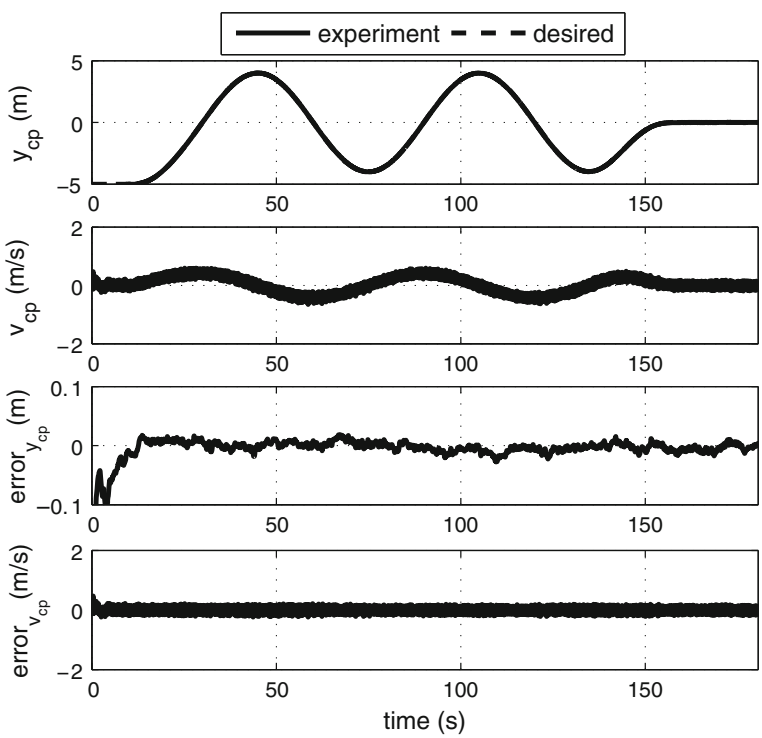

Fig. 21 Position and velocity of the control point in the figure-8 trajectory tracking control

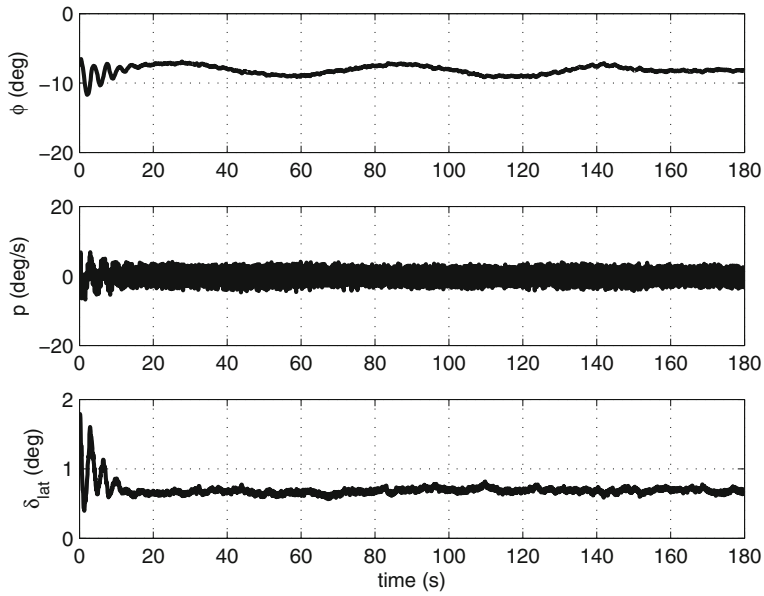

Fig. 22 Closed-loop pitch response and longitudinal cyclic input in the figure-8 trajectory tracking control

desired trajectory with a mean absolute error of 0.7 cm in position and 8.8 cm/s in velocity and stabilizes the lateral motion of the helicopter in the figure-8 trajectory tracking.

Fig. 23 HIL testbed setup for the heading control

5.4 Heading Control Experiment

To test the heading control the helicopter is mounted on the HIL testbed, shown in Fig. 23, with the arm set removed and a flat aluminum plate attached on top of the U-shape plate. The helicopter is then mounted on the flat plate such that its CG is aligned with the vertical axis of the pole as shown in the schematic in Fig. 24. Similar to the previous tests, a constant collective pitch

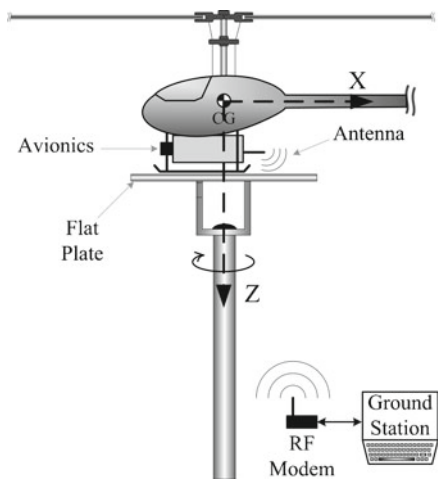

Fig. 24 HIL Testbed schematic for the heading experiment

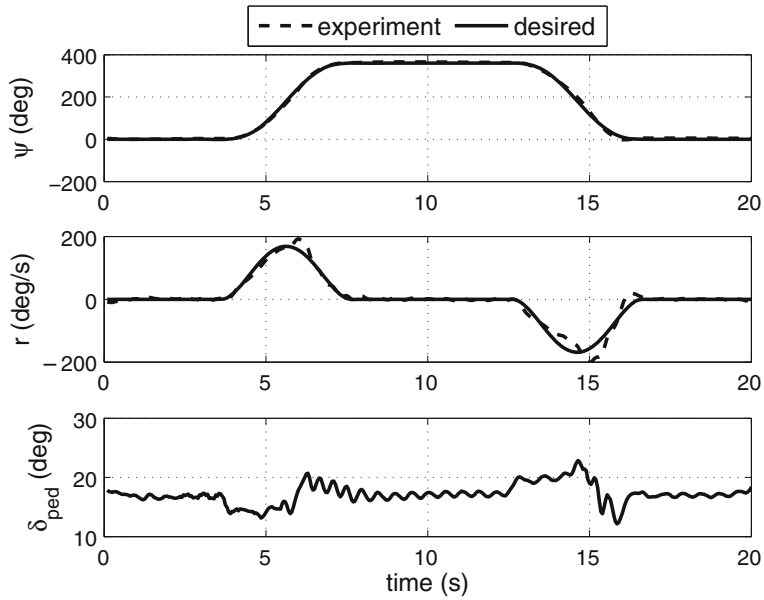

Fig. 25 Closed-loop yaw response to the step trajectory

at hover of $\delta_{col} = 5.6$ deg is maintained after the main blades reached the nominal spinning speed of 1100 rpm. Then, the controller is activated to control the yaw motion of the helicopter to the desired trajectory.

Both a step and a figure-8 yaw trajectory are tested with the results shown in Figs. 25 and 26, respectively. Figure 25 shows the yaw angle, yaw rate and tail command in the yaw control of a fast step trajectory. The results demonstrate that the controller maintains the desired yaw angle (ψ) and yaw rate (r) with a mean absolute error of 4.8 deg and 7.7 deg/s, respectively.

In Fig. 26, during the figure-8 trajectory experiment the helicopter is subject to a large disturbance for the period of 60–80 s. This is done by manually deviating the fuselage away from the desired trajectory. The results in Fig. 26 show that

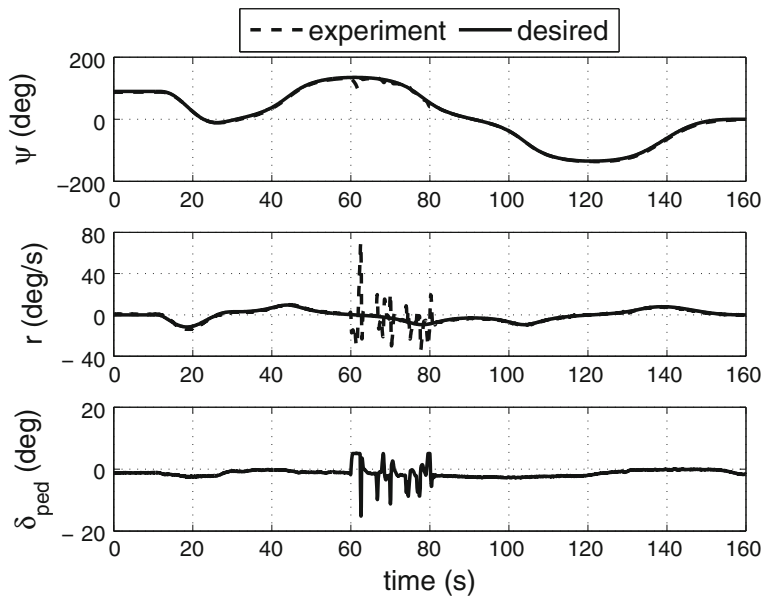

Fig. 26 Closed-loop yaw response to the figure-8 trajectory—the overshoot at about 60 s is due to the external disturbance applied to the helicopter fuselage at 60 s

the controller actuates the pitch of the tail rotor blades to reject the disturbance and maintain the desired yaw angle and yaw rate with a mean absolute error of 2.3 deg and 1.6 deg/s, respectively.

6 Conclusions

A HIL testbed for testing small unmanned helicopters on the ground has been described. The testbed provides a safe and low-cost platform to test a control algorithm in real-time and to tune the control gains. It also allows testing in a controlled environment of the robustness of the controller to external disturbances. To use the testbed a 6-DOF mathematical model of the helicopter is needed to determine the actual motion of the helicopter in the HIL system. This model is described. A small unmanned helicopter is tested on the testbed in three separate experimental tests and detailed results presented. Longitudinal, lateral, and heading control are the three tests. The experiments include: hover, forward, sideways, and figure-8 trajectories for the longitudinal and lateral control and step and figure-8 trajectories for the heading control. The experimental results show that the controller tuned using the HIL testbed achieve a ± 2.5 cm accuracy on the longitudinal and lateral position trajectory tracking, and a ± 5 deg accuracy on the heading trajectory tracking in the presence of external disturbances.

References

1. Merino, L., Caballero, F., Martínez-de Dios, J., Maza, I., Ollero, A.: An unmanned aircraft system for automatic forest fire monitoring and measurement. J. Intell. Robot. Syst. **65**, 533–548 (2012)
2. Casbeer, D., Beard, R., McLain, T., Li, S.-M., Mehra, R.: Forest fire monitoring with multiple small UAVs. In: ACC, vol. 5, pp. 3530–3535 (2005)
3. Li, Z., Liu, Y., Walker, R.A., Hayward, R.F., Zhang, J.: Towards automatic power line detection for a UAV surveillance system using pulse coupled neural filter and an improved hough transform. Mach. Vis. Appl. **21**(5), 677–686 (2009)
4. Marinho, C.A., de Souza, C., Motomura, T., da Silva, A.G.: In-service flare inspection by unmanned aerial vehicles (UAVs). In: 18th World Conference on Nondestructive Testing. Durban, South Africa (2012)
5. Haarbrink, R., Eisenbeiss, H.: Accurate DSM production from unmanned helicopter systems. Int. Arch. Photogramm. Remote Sens. Spat. Inf. Sci. **37**, 1259–1264 (2008)
6. Gundlach, J.: Designing Unmanned Aircaft Systems: A comprehensive Approach, 1st ed. 1801 Alexander Bell Drive, Reston, Virginia 20191-4344, USA: American Istitute of Aeronautics and Astronautics, Inc (2012)
7. Zhang, Y., Chamseddine, A., Rabbath, C., Gordon, B., Su, C.-Y., Rakheja, S., Fulford, C., Apkarian, J., Gosselin, P.: Development of advanced FDD and FTC, techniques with application to an unmanned quadrotor helicopter testbed. J. Franklin Inst. **350**(9), 2396–2422 (2013)
8. Green, W., Oh, P.: Autonomous hovering of a fixed-wing micro air vehicle. In: ICRA, pp. 2164–2169 (2006)
9. Oh, H., Won, D.-Y., Huh, S.-S., Shim, D., Tahk, M.-J., Tsourdos, A.: Indoor UAV control using multi-camera visual feedback. J. Intell. Robot. Syst. **61**, 57–84 (2011)
10. García Carrillo, L., Rondon, E., Sanchez, A., Dzul, A., Lozano, R.: Stabilization and trajectory tracking of a quad-rotor using vision. J. Intell. Robot. Syst. **61**, 103–118 (2011)
11. Mellado-Bataller, I., Pestana, J., Olivares-Mendez, M., Campoy, P., Mejias, L.: MAV work: a framework for unified interfacing between micro aerial vehicles and visual controllers. In: Frontiers of Intelligent Autonomous Systems, ser. Studies in Computational Intelligence, vol. 466, pp. 165–179. Springer Berlin Heidelberg (2013)
12. Chamseddine, A., Zhang, Y., Rabbath, C., Join, C., Theilliol, D.: Flatness-based trajectory planning/replanning for a quadrotor unmanned aerial vehicle. IEEE Trans. Aerospace Electron. Syst. **48**(4), 2832–2848 (2012)
13. Chao, H., Cao, Y., Chen, Y.: Autopilots for small unmanned aerial vehicles: a survey. Int. J. Control Autom. Syst. **8**, 36–44 (2010)
14. Guowei, C., Biao, W., Chen, B., Lee, T.: Design and implementation of a flight control system for an unmanned rotorcraft using RPT control approach. In: 30th Chinese Control Conference (CCC), pp. 6492–6497 (2011)
15. Castillo, C., Moreno, W., Valavanis, K.: Unmanned helicopter waypoint trajectory tracking using model predictive control. In: Mediterranean Conference on Control Automation, pp. 1–8 (2007)
16. Garcia, R.D., Valavanis, K.P.: The implementation of an autonomous helicopter testbed. J. Intell. Robot. Syst. **54**(1–3), 423–454 (2009)
17. Kim, H., Shim, D.H.: A flight control system for aerial robots: algorithms and experiments. Control Eng. Pract. **11**(12), 1389–1400 (2003)
18. Khaligh, S.P., Fahimi, F., Saffarian, M.: Comprehensive aerodynamic modeling of a small autonomous helicopter rotor at all flight regimes. In: AIAA Modeling and Simulation Technologies Conference, pp. 1–10. Chicago, Illinois, United States (2009)
19. Tanaka, K., Ohtake, H., Wang, H.O.: A practical approach to stabilization of a 3-DOF RC helicopter. IEEE Control Syst. Technol. **12**(2), 315–325 (2004)

20. Kutay, A.T., Calise, A.J., Idan, M., Hovakimyan, N.: Experimental results on adaptive output feedback control using a laboratory model helicopter. IEEE Control Syst. Technol. **13**(2), 196–202 (2005)
21. Andrievsky, B., Peaucelle, D., Fradkov, A.L.: Adaptive control of 3-DOF motion for LAAS helicopters benchmark: design and experiments. In: ACC, pp. 3312–3317 (2007)
22. Q.C. Inc.: [Online] Available: http://www.quanser.com (2013). Accessed 5 Mar 2013
23. Montgomery, J.F., Johnson, A.E., Romeliotis, S.I., Matthies, L.H.: The jet propulsion laboratory autonomous helicopter testbed: a platform for planetary exploration technology research and development. J. Field Robot. **23**(3–4), 245–267 (2006)
24. Vitzilaios, N., Tsourveloudis, N.: An experimental test bed for small unmanned helicopters. J. Intell. Robot. Syst. **54**, 769–794 (2009)
25. Whiteman, R.: Training apparatus for remote control model helicopters. U.S. patent US4917610 (1990)
26. Weilenmann, M.F., Geering, H.P.: Test bench for rotorcraft hover control J. Guid. Control Dyn. **17**(4), 729–736 (1994)
27. Narli, V., Oh, P.Y.: A hardware-in-the-loop test rig for desining near-earth aerial robotics. In: Proceedings of the 2006 IEEE International Conference on Robotics and Automation (2006)
28. I. The MathWorks: Online Available: http://www.mathworks.com/ (2013). Accessed 5 Mar 2013
29. Slotine, J.J.E., Weiping, L.: Applied Nonlinear Control. Englewood Cliffs, NJ: Prentice-Hall, Inc. (1991)
30. Fahimi, F., Saffarian, M., The control point concept for nonlinear trajectory-tracking control of autonomous helicopters with fly-bar Int. J. Control **84**(2), 242–253 (2011)